Physicochemical aspects of the mechanisms of rapid antimicrobial contact-killing by sputtered silver oxide thin films under visible light

Tsendzughul, Nathaniel T.; Ogwu, Abraham A.

Published in:
ACS Omega

DOI:
10.1021/acsomega.9b01856

Published: 15/10/2019

Document Version
Publisher's PDF, also known as Version of record

ACS OMEGA

Article

Cite This: ACS Omega 2019, 4, 16847−16859

http://pubs.acs.org/journal/acsodf

Physicochemical Aspects of the Mechanisms of Rapid Antimicrobial Contact-Killing by Sputtered Silver Oxide Thin Films under Visible Light

Nathaniel T. Tsendzughul*,† and Abraham A. Ogwu‡

†School of Computing, Engineering and Physical Sciences, University of the West of Scotland, High Street, Paisley Campus, PA1 2BE Scotland, U.K.

‡East Kazakhstan State Technical University, Ust-Kamenogorsk 070004, Republic of Kazakhstan

ABSTRACT: The morphology and band gap of silver oxide thin films have been tuned by radio frequency reactive magnetron sputtering to deposit transparent, visible-light-activated photocatalytic biomaterials with excellent antimicrobial properties. X-ray diffraction, Raman spectroscopy, and X-ray photoelectron spectroscopy using the Ag $3d_{5/2}$ and Ag $3d_{3/2}$ binding energy peaks have been used to study the chemical composition of the films, and the deposition of two antimicrobial phases of silver oxide, namely, Ag_2O and Ag_4O_4 was confirmed. The optical band gaps of the films were determined by optical spectroscopy and are in the range 2.3 eV (539.6 nm) to 3.2 eV (387.8 nm). Strong transmission of up to 80% was observed in the visible region around 650−750 nm. Silver ion release on the surfaces of the films was monitored using atomic absorption spectroscopy, and sustained silver ion release in both water and saline solution for 24 h was confirmed. Nanocrystallites of sizes between 2.45 and 31.30 nm were observed on the surfaces. The films were challenged with two Gram-positive bacteria (*Staphylococcus aureus* and *Staphylococcus epidermidis*) and two Gram-negative bacteria (*Escherichia coli* and *Pseudomonas aeruginosa*) during antimicrobial activity tests using killing curve analysis with 100% contact killing recorded in 25 and 5 min, respectively. The mechanism of antimicrobial efficacy is suggested to be due to silver ion release, small crystallites, and the ease of ligand replacement in the silver oxide stoichiometry, their exchange and interactions of ligands in the microbe's biological systems. Our current finding opens the door to furthering the development of visible-light-activated antimicrobial surfaces.

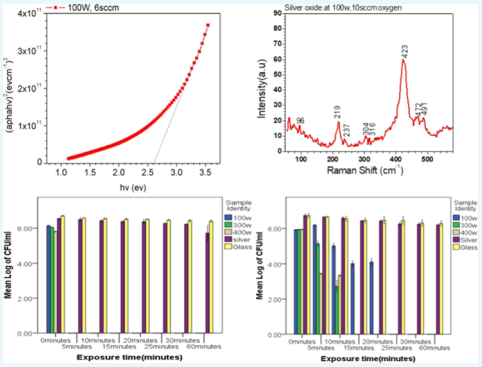

1. INTRODUCTION

The sustained fight against pathogenic microorganisms due to their negative effect on living matter has been on for ages. Scientists and researchers from different fields are engaged with this process, and several tools have been used over the years to offer a solution to this problem. The introduction of antibiotics in the early 20th century was a major game changer in the fight against microorganisms. Recently, however, resistance of microbial infections to multiple antibiotic treatments has been reported. Resistant bacterial species, also referred to as superbugs, are classified into three categories, namely, the critical, high, and medium resistance groups. This situation has therefore led to the need to develop antimicrobial thin film coatings that can effectively deal with this problem especially on surfaces in hospital environments like medical textiles, medical equipment like catheters, and medical implants under visible-light-activated photocatalysis.[1] The most promising materials evaluated to date for this application include silver nitride and oxynitride films prepared by reactive magnetron sputtering and activated with indoor visible light photocatalysis reported by Rtimi et al.[2,3] Leyland et al.[4] have also recently (2017) reported doping titanium dioxide coatings with copper and fluorine using sol and dip coating to prepare a visible-light-activated antimicrobial coating.

Metals play vital roles in the structure, function, and dynamics of biological systems.[5−7] Phosphorus is essential in both the DNA double helix and cell energetics in adenosine triphosphate.[8−12] The electrical flux generated due to the movement of sodium and potassium ions across the cell membrane transmits information in the nervous system.[6,7] Metals were extensively used for disinfection and antimicrobial treatment before the advent of antibiotics.[13,14] Metals can be replaced with coordination complexes of biological systems and therefore used to alter their structure, function, and dynamics.

Transition metals such as gold, silver, copper, and titanium have been used as antimicrobials either as metals, alloys, or oxides due to the peculiarity of their chemistry.[15] Copper and its oxides have demonstrated good antimicrobial properties being reported as effective antimicrobials with the capacity of killing up to 99.9% of bacteria in contact with them in approximately 2 h.[16,17]

Received: June 21, 2019
Accepted: September 12, 2019
Published: October 2, 2019

For an antimicrobial material to be effective, it must have the ability to cause multiple attack on microbes. A simultaneous attack on the cell wall, DNA, and protein synthesis destroys the bacteria's defense, leaving little room for resistance.[18−20]

The generation of electron−hole pairs in semiconductors through the photocatalytic process provides potent antimicrobial properties. In addition, the production of reactive oxygen species (ROS) and hydroxyl radicals as well as metal ion release provides the necessary tools for killing microbes.[21]

Titanium dioxide has been extensively researched and used as a photocatalyst due to its low cost, easy availability, and photochemical stability.[22,23] It however has a band gap of about 3.1 eV and is excited using ultraviolet light, which imposes a limitation in its utilization for some applications.[24] Some of the approaches used to obtain visible-light-activated photocatalysts include doping of titanium dioxide and dye sensitization.[25−28] The development of a photocatalyst that is an undoped single compound, cheap enough, and activated using visible light has remained a major challenge to date.

The band gap and morphology of semiconductor thin films can be tuned using deposition parameters such as oxygen flow rate, forward power, and chamber temperature during deposition. In this investigation, the band gap and morphology of a multiphase but undoped single compound silver oxide thin film was varied using reactive magnetron sputtering and two parameters, the forward power and oxygen flow rate, during deposition using the conditions shown in Table 1, to obtain a semiconductor biomaterial that is optically transparent, photocatalytic under visible light, and has antimicrobial properties. The previous investigations on photocatalytic silver oxide films were based mainly on the dissociation of dyes,[26−28] while our present investigation is focused on their antimicrobial killing effect on the microbes investigated in this paper.[29] Silver oxide photocatalysts have been investigated and reported to be very stable after eight cycles of use on methyl orange, phenols, and methyl blue.[30]

Table 1. Deposition Conditions for the Prepared Silver Oxide Thin Films

argon flow rate (sccm)	30, 60
oxygen flow rate (sccm)	0, 2, 4, 6, 8, 10
forward radio frequency (rf) input power (W)	100, 200, 250, 300, 350, 400
reflected power (W)	<2
target	silver
substrate	glass
deposition time (min)	2 or 5
substrate temperature	room temperature

2. RESULTS

2.1. Deposition Conditions. The deposition conditions used to produce the silver oxide thin films are presented in Table 1

The thickness of the silver oxide films deposited increased with deposition power. The average thicknesses of a selection of films were measured by scanning electron microscopy (SEM) and are presented in Table 2. The rate of deposition of the oxides of silver varies with forward deposition power, and typical values are presented in Table 2.

2.2. Scanning Electron Microscopy Results. Scanning electron microscope micrographs of the cultured bacteria on silver oxide thin film are shown in Figure 1.

Table 2. Selected Typical Thicknesses and Deposition Rates for Our Silver Oxide Films Prepared Using 5 min Deposition Time

s/no	forward power (W)	oxygen flow rate (sccm)	thickness (nm)	deposition rate (nm/min)
1	100	6	116.00 ± 2.25	23.20
2	200	6	144.75 ± 2.75	28.95
3	300	6	333.60 ± 3.64	66.70

2.3. X-ray Diffraction (XRD) Analysis. The XRD spectra for the as-deposited thin films are shown in Figure 2A.

Both silver and its oxides AgO and Ag_2O previously reported in the literature are observed in our analysis.[14,29] Dellasega et al.[31] also previously reported observing tetragonal and monoclinic antimicrobial phases of Ag_4O_4 in their silver oxide films. We observed the Ag_4O_4 phase in our XRD spectra of the films deposited at a forward power of 100 W and an oxygen flow rate of 10 sccm as reported by Dellasega.[32] We also detected Ag_2O in our films produced at 400 W forward power.[33]

The crystal sizes of the deposited silver oxide thin films were calculated using the Schuler formula[34]

$$D = \frac{0.89\lambda}{\beta \cos\theta} \quad (1)$$

where D is the crystal size, λ is the wavelength of X-rays (Cu Kα = 1.54 Å), θ is calculated from the 2θ angle, and β is the full width at half-maximum (FWHM). The full width at half-maximum was obtained by Gaussian−Lorentzian fitting of the XRD spectra using Magic plots software. The crystallite sizes are presented in Table 3.

2.4. Raman Spectroscopy. The details of the phases observed in our Raman analysis for films prepared at 100 W forward power are shown in Table 4.

The major phases in our deposited films are AgO, Ag_2O, and Ag_4O_4 for the films prepared at 100 W forward power. The same phases were observed for all of the films we prepared between 100 and 400 W forward power, although additional Raman peaks associated with these phases were observed. A typical Raman spectrum obtained in our investigation is shown in Figure 2B. The irreducible representation from group theory was used to predict vibrational modes that are Raman-active. The irreducible representation of silver oxides indicates that Ag_2O has the following vibrational modes[33]

$$\Gamma_{3N} = A_{2u} + E_u + 3T_{1u}(IR) + T_{2u} + T_{2g}(R) \quad (2)$$

The analysis predicts three active modes like the prediction for the Cu_2O structure. The $3T_{1u}$ modes are infrared-active, while the T_{2g} mode is Raman-active. The T_{1u} symmetry infrared-active modes are due to relative motion of the silver and oxygen lattices and are responsible for the asymmetric Ag−O stretching mode as well as the asymmetric O−Ag−O bending mode vibrations observed. The T_{2g} Raman active mode about the symmetry center at Ag(I) is generated by the O_2^- ions and is assigned to Ag−O stretching vibration. The Ag_2O phase of silver oxide does not display Raman and infrared activity due to its inversion symmetry.

The nature of the optically active vibrational modes for monoclinic AgO was established using factor group analysis. The C_{2b} factor group and the two Ag(III) and two Ag(I) ions in the primitive cell sites of C_1 symmetry and four O^{2-} ions in the C_1 sites are used for establishing the vibrational modes of silver oxide.[33] The vibrational modes resulting from the analysis are

DOI: 10.1021/acsomega.9b01856
ACS Omega 2019, 4, 16847−16859

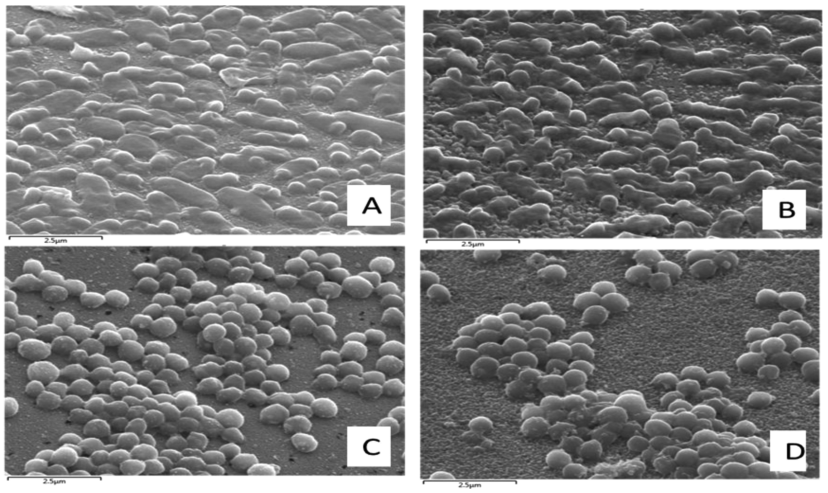

Figure 1. Scanning electron microscope images of (A) *Escherichia coli*, (B) *Pseudomonas aeruginosa*, (C) *Staphylococcus aureus*, and (D) *Staphylococcus epidermidis* on silver oxide surfaces.

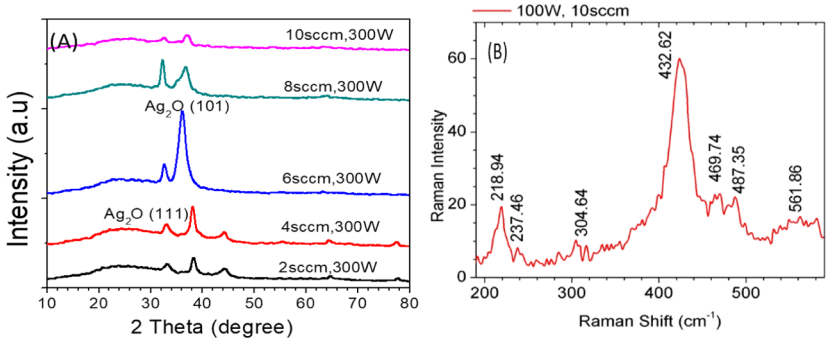

Figure 2. (A) XRD spectra of silver oxides deposited at different oxygen flow rates at 300 W forward power and (B) Raman spectrum of silver oxide deposited at 100 W power and 10 sccm oxygen flow.

Table 3. Crystallite Sizes of Silver Oxides at Varying rf Powers and Oxygen Flow Rates

rf power (W)	oxygen flow (sccm)	2θ	θ	cos θ	FWHM (deg)	FWHM (rad)	D (m)
200	2	38.23	19.115	0.944863	1.773	0.030945	4.69×10^{-09}
		44.35	22.175	0.926035	1.773	0.030945	4.78×10^{-09}
	8	36.48	18.24	0.949754	2.5938	0.04527	3.19×10^{-09}
		63.37	31.685	0.850949	3.7692	0.065785	2.45×10^{-09}
250	6	32.35	16.175	0.960415	1.1812	0.020616	6.92×10^{-09}
		35.8	17.9	0.951594	2.803	0.048922	2.94×10^{-09}
	8	36.48	18.24	0.949754	2.5938	0.04527	3.19×10^{-09}
		63.37	31.685	0.850949	3.7692	0.065785	2.45×10^{-09}
300	8	32.23	16.115	0.960707	2.9316	0.051166	2.79×10^{-09}
		36.89	18.445	0.948628	2.9316	0.051166	2.82×10^{-09}
	10	32.53	16.265	0.959977	2.1344	0.037252	3.83×10^{-09}
		37.09	18.545	0.948074	2.1344	0.037252	3.88×10^{-09}
400	2	33.21	16.605	0.958298	2.9572	0.051613	2.77×10^{-09}
		38.34	19.17	0.944548	2.9572	0.051613	2.81×10^{-09}
		43.9	21.95	0.92751	2.9572	0.051613	2.86×10^{-09}
	6	35.97	17.985	0.951137	3.0602	0.053411	2.7×10^{-09}
		38.07	19.035	0.94532	3.0602	0.053411	2.71×10^{-09}

$$\Gamma_{vib} = 8A_u(IR) + 7B_u(IR) + 3A_g(R) + 3B_g(R) \quad (3)$$

Monoclinic AgO is found to have 21 optically active modes, 15 of which are infrared-active and 6 are Raman-active.[33]

2.5. X-ray Photoelectron Spectroscopy (XPS). The XPS survey and deconvoluted high-resolution spectra for the deposited samples are shown in Figure 3.

The XPS analysis of the samples indicates the presence of mixed phases of silver oxides Ag_2O and AgO in silver, which agrees with both XRD and Raman analyses conducted on the samples. The XPS core-level binding energies of around 374 eV[35] corresponding to silver were observed to be present in all of the samples, confirming the observation of strong absorption spectrum of the sample reported at about 370 nm in optical

DOI: 10.1021/acsomega.9b01856
ACS Omega 2019, 4, 16847−16859

Table 4. Selected Raman Spectra Peak Point Data Used for the Identification of the Phases in the Silver Oxide Thin Films Deposited at 100 W Forward Power and 10 sccm Oxygen Flow Rate

forward power (W) during deposition	Raman peaks (cm^{-1})	FWHM	identified phases
100	467	12.12	AgO, Ag_4O_4
100	486	18.48	AgO, Ag_4O_4
100	424	28.76	Ag_4O_4
100	217	26.38	AgO, Ag_4O_4
100	423	29.06	Ag_2O, Ag_4O_4
100	477	32.06	Ag_2O, Ag_4O_4

spectrophotometry of the samples. The silver associated with AgO was observed to be at a binding energy of 367.1 eV,[36] suggesting the presence of a mixture of Ag and AgO (Figure 3C). Silver associated with Ag_2O is reported at a binding energy of 367.7 eV, implying the mixture of the two in the sample. The O 1s binding energies in the high-resolution spectra of oxygen are reported in the literature to belong to AgO and Ag_2O, while some are assigned to superoxide, hydroxyl and carbonate groups. The presence of superoxide and hydroxyl groups confirms the antimicrobial properties of the oxides since the presence of these groups is very potent against bacteria.[37] The O 1s peak in AgO was observed at 530.1 eV, in agreement with earlier literature report,[38] confirming the presence of this phase in the sample, while the binding energy observed at 528.6 eV is due to Ag_2O[39,40] in the sample as shown in Figure 3B. The presence of the O 1s peaks at binding energies between 530 and 532 eV is indicative of the presence of carbonates, superoxide, and hydroxyl group.[41,42]

2.6. Optical Transmittance, Reflectance, and Band Gap. Optical transmittance and reflectance for the as-deposited silver oxide thin films were measured in the 350−1100 nm wavelength range using the Aquila nkd-8000 spectrophotometer. The Aquila optical spectrophotometer was calibrated using fused silica, which also served as the reference for the optical measurements. A plot of absorption and transmittance spectra as well as the absorption coefficient versus wavelength or photon energy for direct band gap for each sample was generated for silver oxide. The thicknesses of the deposited films were measured using an image analysis software attached to the scanning electron microscope. The optical spectrophotometer measurements on our prepared silver oxide thin film samples indicated that the silver oxides transmit up to 80% of light incident in the wavelength range between 650 and 750 nm, which is in the visible region as presented in Figure 4A−C.

The transmission spectrum was generated from the equation[43]

$$T = \frac{I}{I_0} \tag{4}$$

where I_0 and I are the intensities of the incident and transmitted light beams, respectively. The absorption coefficient was plotted using the relationship[44]

$$\alpha = \frac{1}{d}\log\left(\frac{I_0}{I}\right) \tag{5}$$

which links the optical absorption coefficient (α) and thickness (d).

Tauc's relation[45] expressed in eq 6 was used to determine the band gap of the thin films

$$(\alpha h\nu) = A(h\nu - E_g)^{1/2} \tag{6}$$

where h is Planck's constant, ν is the photon frequency, and E_g is the optical band gap.

Tauc plots were generated, and the linear portion of the curves was extrapolated to the $h\nu$ axis to give an estimate of the band gap. The direct optical band gap to the first approximation is a straight line, which when extrapolated touches the photon energy axis at the band gap value. The typical plot obtained is as shown in Figure 4A. The band gap values obtained were

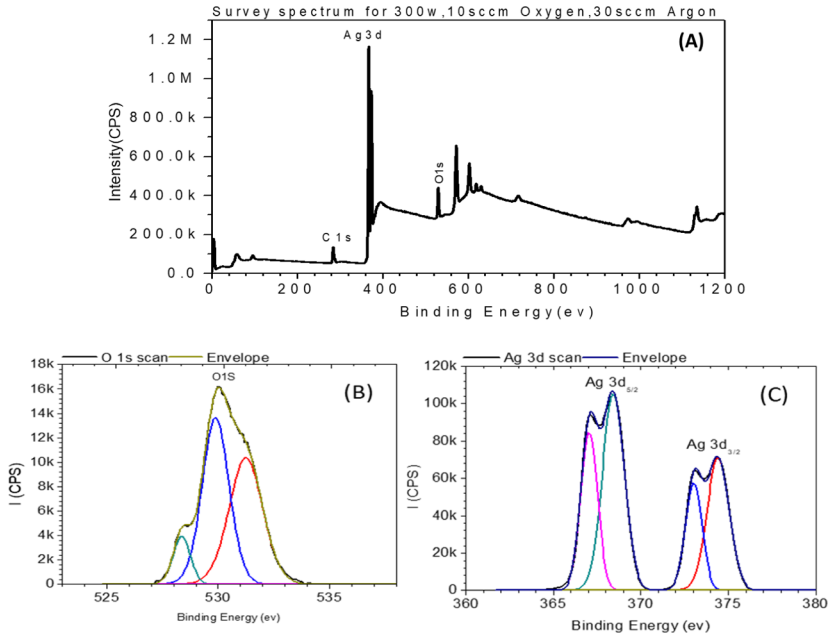

Figure 3. XPS binding energy spectra of samples deposited at 300 W power and 10 sccm oxygen: (A) survey, (B) oxygen high-resolution, and (C) silver Ag 3d spectra.

DOI: 10.1021/acsomega.9b01856
ACS Omega 2019, 4, 16847−16859

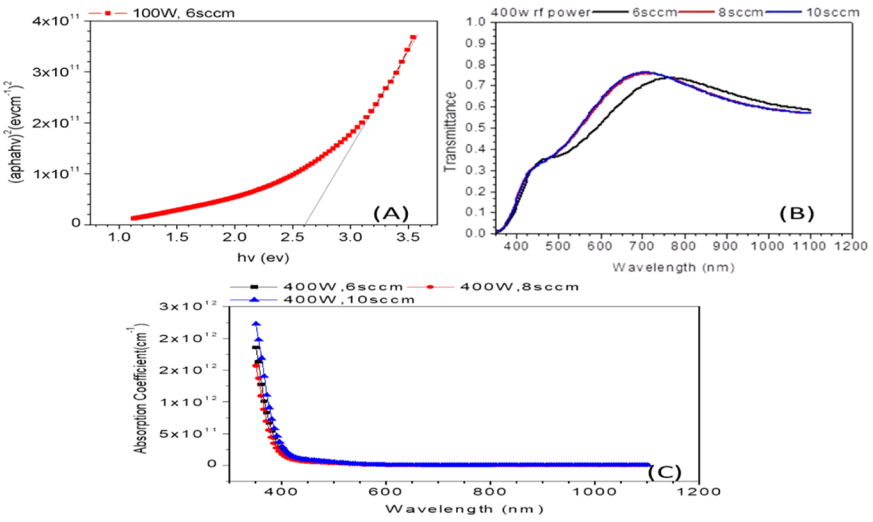

Figure 4. (A) Tauc plot for silver oxide deposited at 100 W power and 6 sccm oxygen flow, (B) transmittance spectrum of silver oxide deposited at 400 W and 10, 8, and 6 sccm oxygen flow, and (C) absorption coefficient as a function of wavelength for silver oxides deposited at a power of 400 W and varied oxygen flow rates of 10, 8, and 6 sccm.

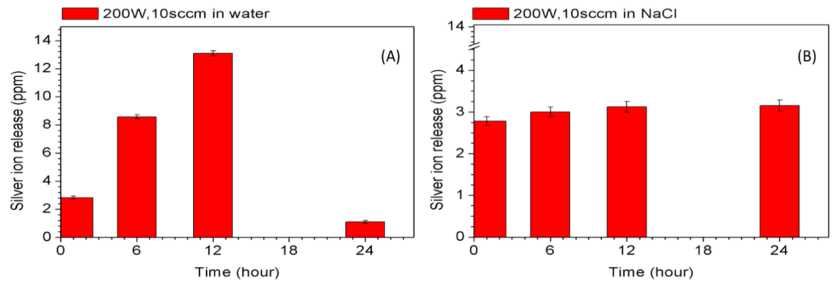

Figure 5. Silver ion release from silver oxide deposited at 200 W power and 10 sccm oxygen flow in (A) water and (B) saline solution.

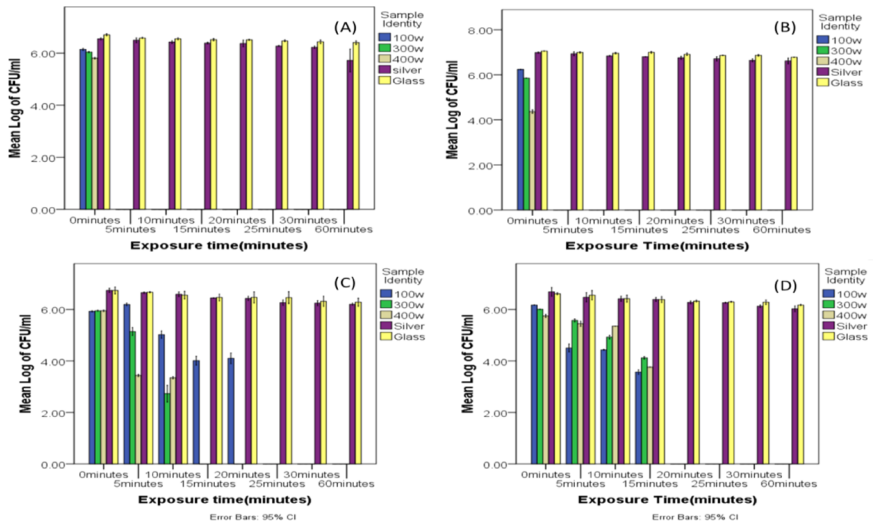

Figure 6. Killing curve for bacteria on silver oxides deposited at 100, 300, and 400 W forward powers each at 10 sccm oxygen flow, silver at 300 W, and glass slide for (A) *E. coli*, (B) *P. aeruginosa*, (C) *S. aureus*, and (D) *S. epidermidis*.

between 2.3 eV (539.6 nm) and 3.1 eV (387.8 nm) depending on deposition conditions used for preparing the silver oxide films and span both the ultraviolet and visible ranges of the solar spectrum, consistent with other reports in the literature.[46−48] The silver oxides can therefore be activated as photocatalysts using visible light and thus eliminating the use of ultraviolet radiation for activation. It was also observed that the silver oxides deposited absorbed solar radiation at about 370 nm as shown in Figure 4C.

2.7. Atomic Absorption Spectroscopy. Silver ion release was observed in both water and saline solution as shown in Figure 5A,B.

The ion concentration in water was observed to be higher than that in saline solution. The lowest concentration of 0.5343

DOI: 10.1021/acsomega.9b01856
ACS Omega 2019, 4, 16847−16859

Table 5. Student's *t*-Test Statistical Analysis for Gram-Negative *E. coli* and *P. aeruginosa*

bacteria	samples compared	mean	stand. dev.	two-tailed sig.	significance
E. coli	100 W	0.7682	2.17292		
	vs			0.991	no sig. diff.
	300 W	0.7554	2.13654		
	100 W	0.7682	2.17292		
	vs			0.969	no sig. diff.
	400 W	0.7261	2.05381		
	300 W	0.7554	2.13654		
	vs			0.978	no sig. diff.
	400 W	0.7261	2.05381		
	100 W	0.7682	2.17292		
	vs			0.000	sig. diff.
	silver	6.3078	0.25923		
	300 W	0.7554	2.13654		
	vs			0.000	sig. diff.
	silver	6.3078	0.25923		
	400 W	0.7261	2.05381		
	vs			0.000	sig. diff.
	silver	6.3078	0.25923		
	100 W	0.7682	2.17292		
	vs			0.000	sig. diff.
	glass	6.5236	0.09464		
	300 W	0.7554	2.13654		
	vs			0.000	sig. diff.
	glass	6.5236	0.09464		
	400 W	0.7261	2.05381		
	vs			0.000	sig. diff.
	glass	6.5236	0.09464		
Pseudomonas	100 W	0.7798	2.20557		
	vs			0.965	no sig. diff.
	300 W	0.7317	2.06945		
	100 W	0.7798	2.20557		
	vs			0.809	no sig. diff.
	400 W	0.5459	1.54403		
	300 W	0.7317	2.06945		
	vs			0.842	no sig. diff.
	400 W	0.5459	1.54403		
	100 W	0.7798	2.20557		
	vs			0.000	sig. diff.
	silver	6.7864	0.13170		
	300 W	0.7317	2.06945		
	vs			0.000	sig. diff.
	silver	6.7864	0.13170		
	400 W	0.5459	1.54403		
	vs			0.000	sig. diff.
	silver	6.7864	0.13170		
	100 W	0.7798	2.20557		
	vs			0.000	sig. diff.
	glass	6.9269	0.09077		
	300 W	0.7317	2.06945		
	vs			0.000	sig. diff.
	glass	6.9269	0.09077		
	400 W	0.5459	1.54403		
	vs			0.000	sig. diff.
	glass	6.9269	0.09077		

ppm was recorded for silver oxide deposited at 400 W power after exposure for 12 h, and the highest value of 33.0152 ppm was observed for silver deposited at 300 W after exposure for 24 h. The silver oxide deposited at 200 W showed a low ion release in the first 1 h, which builds up to higher values after 6 and 12 h. The results indicate that silver ions are released in both water and saline solution and that the release is sustained for 24 h, which confirms that the silver oxide thin films can function as antimicrobial material surfaces. The availability of silver ions on the surfaces to both initiate and sustain antimicrobial activity in

DOI: 10.1021/acsomega.9b01856
ACS Omega 2019, 4, 16847−16859

water or saline solution is guaranteed. The silver ions released in water and saline solutions can then attach to bacteria or penetrate the bacteria, leading to a disruption of the chemical structure and function of the biochemical components inside the bacteria.

2.8. Results of Antimicrobial Tests and Killing Curves for Microbes. The results obtained are as shown in Figure 6A–D representing the killing curves for the microbes we investigated after the exposure of bacteria at different time intervals to silver oxide, silver, and microscope glass slide control surfaces, respectively.

2.9. Statistical Analysis. A Student's *t*-test statistical analysis was performed with the surfaces as independent variables while the log of colony forming units (CFUs) was the dependent variable, and the result is presented in Tables 5 and 6 for Gram-negative and Gram-positive bacteria, respectively.

No statistically significant differences in the means of the log of colony forming units was observed between the silver oxide surfaces prepared at 100, 300, and 400 W forward power during deposition for all of the four microbes under study. There was no statistically significant difference in the mean of log of the colony forming units as indicated below

(1) *E. coli*: 100 vs 300 W ($p > 0.991$); 100 vs 400 W ($p > 0.969$); 300 vs 400 W ($p > 0.978$).
(2) *P. aeruginosa*: 100 vs 300 W ($p > 0.965$); 100 vs 400 W ($p > 0.809$); 300 vs 400 W ($p > 0.842$).
(3) *S. aureus*: 100 vs 300 W ($p > 0.494$); 100 vs 400 W ($p > 0.419$); 300 vs 400 W ($p > 0.913$).
(4) *S. epidermidis*: 100 vs 300 W ($p > 0.884$); 100 vs 400 W ($p > 0.906$); 300 vs 400 W ($p > 0.978$).

Statistically significant differences were observed between the means of the colony forming units for each of the four bacteria on all silver oxide-coated substrates compared with the control silver-coated and the uncoated glass substrates over the time considered. The details of the findings for each microbe are as follows:

(1) *E. coli*: All comparisons between silver oxides (prepared at 100, 300 and 400 W) at 10 sccm oxygen flow and the control surfaces (silver, glass) indicated a statistically significant difference in the means of the colony forming units, and all were at $p < 0.05$ level of significance.
(2) *P. aeruginosa*: A similar pattern observed in *E. coli* was observed for this microbe. All comparisons between silver oxides (prepared at 100, 300, and 400 W) at 10 sccm and the control surfaces (silver and glass) indicated a statistically significant difference in the means of the colony forming units, and all were at $p < 0.05$ level of significance.
(3) *S. aureus*: The microbial colonization levels for the silver oxide-coated substrates compared to the silver-coated and uncoated glass substrates were all at $p < 0.001$ level of statistical significance.
(4) *S. epidermidis*: The microbial colonization levels for the silver oxide-coated substrates compared to the silver-coated and uncoated glass substrates were all at $p < 0.001$ level of statistical significance.

One-way analysis of variance (ANOVA) was conducted on the data obtained from the killing curve measurements to test whether there was any significant difference between the means of the log of colony forming units with time at different time intervals on samples at different deposition conditions. The level of significance was set at 0.05 or 5%. The null hypothesis set was that there is always no significant difference between the means of the log of colony forming units for bacteria in contact with

Table 6. Student's *t*-Test Statistical Analysis for Gram-positive *S. aureus* and *S. epidermidis*

bacteria	samples compared	mean	stand. dev.	two-tailed sig.	significance
S. aureus	100 W	2.6851	2.88939		
	vs			0.494	no sig. diff.
	300 W	1.7278	2.54687		
	100 W	2.6851	2.88939		
				0.419	no sig. diff.
	400 W	1.5913	2.33373		
	300 W	1.7278	2.54687		
	vs			0.913	no sig. diff.
	400 W	1.5913	2.33373		
	100 W	2.6851	2.88939		
	vs			0.008	sig. diff.
	silver	6.4450	0.20053		
	300 W	1.7278	2.54687		
	vs			0.001	sig. diff.
	silver	6.4450	0.20053		
	400 W	1.5913	2.33373		
	vs			0.001	sig. diff.
	silver	6.4450	0.20053		
	100 W	2.6851	2.88939		
	vs			0.007	sig. diff.
	glass	6.4848	0.16349		
	300 W	1.7278	2.54687		
	vs			0.001	sig. diff.
	glass	6.4848	0.16349		
	400 W	1.5913	2.33373		
	vs			0.001	sig. diff.
	glass	6.4848	0.16349		
S. epidermidis	100 W	2.3760	2.63728		
	vs			0.884	no sig. diff.
	300 W	2.5786	2.80863		
	100 W	2.3760	2.63728		
	vs			0.906	no sig. diff.
	400 W	2.5385	2.77604		
	300 W	2.5786	2.80863		
	vs			0.978	no sig. diff.
	400 W	2.5385	2.77604		
	100 W	2.3760	2.63728		
	vs			0.004	sig. diff.
	silver	6.3282	0.20775		
	300 W	2.5786	2.80863		
	vs			0.007	sig. diff.
	silver	6.3282	0.20775		
	400 W	2.5385	2.77604		
	vs			0.006	sig. diff.
	silver	6.3282	0.20775		
	100 W	2.3760	2.63728		
	vs			0.004	sig. diff.
	glass	6.3794	0.14425		
	300 W	2.5786	2.80863		
	vs			0.006	sig. diff.
	glass	6.3794	0.14425		
	400 W	2.5385	2.77604		
	vs			0.006	sig. diff.
	glass	6.3794	0.14425		

DOI: 10.1021/acsomega.9b01856
ACS Omega 2019, 4, 16847−16859

surfaces. Results obtained from the ANOVA test indicate that the p values for all of the four microbes were less than 0.05, implying that at least there is a pair of data set whose means are significantly different from each other, thus justifying the conduct of the post hoc Tukey test to find out which pair has statistically significant difference in the means of log of colony forming units. A post hoc Tukey test was therefore conducted, which confirmed that the means of their colony forming units on the tested surfaces were statistically significantly different ($p < 0.05$). Our investigation shows that the silver oxide surfaces are antimicrobial with the capacity to kill the microbes examined in this investigation within a maximum of 20 min of exposure to the silver oxide surfaces as shown in Figure 5a−d. *E. coli* and *P. aeruginosa* are unable to survive on the silver oxide surface for more than 5 min, *S. aureus* survives between 10 and 15 min, and *S. epidermidis* survives up to a maximum of 20 min. The microbes however continue to grow on both the silver and the uncoated microscope glass slide control surfaces up to 60 and 90 min after exposure, respectively.

3. DISCUSSION

Wang et al.[46] and other researchers[30,47,48] proposed the following basic reaction mechanisms for the photocatalytic dissociation of chemical dyes using Ag_2O in the visible light regime on different chemical dyes including methyl orange. The process starts with the irradiation of Ag_2O with light energy lower than or equal to its band gap energy of 1.9 eV, leading to the generation of electron−hole pairs that migrate to the surface, i.e.

$$Ag_2O + h\nu \rightarrow h^+ + e^- \quad (7)$$

In an aqueous environment, the electron−hole pairs will react with oxygen to form reactive oxygen species (ROS), hydroxyl radicals $^{\bullet}OH$, and superoxide anions as indicated below

$$O_2 + 2^{\bullet}OH + 2h^+ \rightarrow O_3 + H_2O \quad (8)$$

$$O_3 + e^- \rightarrow O_3^- \quad (9)$$

The photocatalytic dissociation of chemical dyes through the above reaction mechanisms will involve the following reactions

$$h^+ + \text{dye} \rightarrow \text{oxidation products} \quad (10)$$

$$O_3^- + \text{dye} \rightarrow \text{oxidation products} \quad (11)$$

The above reaction pathways for silver oxide exposed to an aqueous environment are also supported by density functional theory calculations.[30] The above photocatalytic dissociation in combination with silver ion release in solution confirmed by our atomic absorption spectroscopic measurements and the nano-sized particles evaluated from X-ray diffraction analysis provides the necessary chemical entities for the antimicrobial interaction of silver oxide with microbes as discussed below.

These results from the antimicrobial tests agree well with the earlier results from ion release, XPS, Raman, XRD, and optical characterization measurements, which confirmed that the silver oxides are photocatalytic and contain antimicrobial silver oxide phases and crystallite sizes between 2.45 and 31.30 nm. The results also indicate potentially that the silver oxides are better antimicrobial materials compared to silver, which is also reported to be antimicrobial. The nanocrystallites are small enough to pass through the pores in the bacterial cell membrane, which are 2−3 nm,[49,50] resulting in a simultaneous attack on inner biochemical components such as DNA/RNA and proteins, while the other crystallites attack the cell membrane. This multiple attack does not permit the bacteria to develop resistance against the attack. The band gap of the mixed-phase silver oxide materials, which ranges between 2.3 and 3.1 eV, is also in the visible region of the solar spectrum, suggesting that the material can be activated using sunlight. Our antimicrobial tests were carried out under ordinary sunlight under room conditions in the absence of ultraviolet lamps, and the killing effect was quite pronounced for both Gram-positive and Gram-negative bacteria.

The killing mechanism of the bacteria exposed to silver oxide films in our investigation is believed to be affected by an initial photocatalytic dissociation into silver ions, reactive oxygen, superoxide, and hydroxyl radicals. The presence of these radicals and silver ions confirmed by our ion release measurements in solution in an aqueous environment leads to ligand and metal complex replacements in the cell membrane, DNA, and proteins in the bacteria and the killing of the bacteria as previously reported.[29]

It has been established that silver ions interact with the cell wall, resulting in antimicrobial activity. The interaction with the cell wall paves the way for penetration of silver-containing species into the interior of the cell to interact with biochemical components such as DNA and enzymes. Holt and Bart[51] reported that *E. coli* when exposed to silver ions permitted 60% transportation of the ions into the interior of the cell, while 40% interacted with the cell membrane. This interaction causes lysis and detachment of the cell membrane from the cell wall as well as creates an electron-light region, which originally was dense, resulting in loss of replication ability of the bacteria.[52]

Atomic silver (Ag^0) is inert, but the ionic forms Ag^+ and Ag^{2+} are reactive. The Ag^+ ion with its d^{10} electronic configuration has zero-ligand field stabilization energy and readily forms labile complexes in which there is rapid exchange of the original ligand set for new ligands available from the surrounding system. Ligand-exchange reactions have suggested the relative order of Ag^+ bond strength to be[52−58]

$$Ag{-}P > Ag{-}S \gg Ag{-}Cl > Ag{-}N \gg Ag{-}O$$

The mechanism of the antimicrobial activity of silver is observed to involve three interactions, namely,

(1) the inhibition of transport functions in the cell wall, which affects respiration
(2) the interruption of cell metabolism by changing the enzyme structure, and
(3) inhibition of cell division in its interaction with DNA.[52−58]

This multiple attack of silver ions on microbes is very effective and unique and reduces the possibility of resistance development by microbes.[52−58] Several significant structural and morphological changes occur in bacteria after exposure to silver ions such as an electron-light region observed in the center of the cell containing a tightly condensed substance twisted together, a big gap between the cytoplasmic membrane and the cell wall, and the presence of some electron-dense granules around the cell wall.[52,54] The DNA is effectively replicated when DNA molecules are in a relaxed state, but the replication ability is lost when DNA cells are condensed, and this happens when silver ions penetrate the bacterial cell wall. This subsequently results in the death of the bacterial cell. Protein groups are also inactivated when heavy metals react with proteins by attachment. In this interaction, silver inhibits the uptake of phosphate and the

DOI: 10.1021/acsomega.9b01856
ACS Omega 2019, 4, 16847−16859

release of phosphate mannitol, succinate, proline, and glutamine in *E. coli*. The antimicrobial activity of the silver(I)-based complexes is controlled by the weak binding property of the Ag−O bond and accounts for the ease of ligand replacement in the complex. In biological system, the ease of ligand replacement in the silver (I) complexes would result in further replacement with biological ligands. Ligand replacement is observed for O^-, N^-, and S^- donor atoms. The weak Ag−O and Ag−N bonds exhibit antimicrobial and antifungal activities, while the major inhibitors of bacteria and yeast growth are the sulfur atoms in proteins. The silver(I) ion freely interacts with ligands in proteins, enzymes, and cell membranes, which have a rich supply of the donor atoms replacing them and resulting in the antimicrobial activity of the complex.[53] Silver(I) ions are released into the biological system by coordinating ligands in the silver(I) complex. The efficacy of the antimicrobial activity of the complex is defined by the ease of ligand replacement in the complex. According to Tajmir-Riahi et al.,[55] Ag(I) binds very strongly with nucleic acids, resulting in the formation of many complexes with the DNA. Type I complexes result when silver binds with guanine and adenine at the N7 site at low and high concentration ratios of Ag and nucleotide. Type II complexes are formed between the Ag(I) ion and G−C and A−T base pairs. The antimicrobial and other desirable properties of the complexes can be changed by varying the type and number of ligands coordinating with the Ag(I) ion in the complex.[56] Some of the key factors used in the design of silver-based antimicrobial complexes are as follows:[56]

(1) The type of atoms bound to the Ag^+ ion.
(2) The ease of ligand replacement and control of Ag^+ ion release.
(3) Chemical and photostability.
(4) Cost.

The bonding between the silver ion, Ag^+, and enzymes available in the bacterial respiratory chain initiates the production of reactive oxygen species in large quantities due to inefficient electron passage at the terminal oxidase, providing an explanation as to why the silver(I) ion is toxic to bacteria. The rate of metal ion release and the relative stability of any silver complexes can be controlled using variations in the ligand architecture and the overall structural motif of the compound.

Izatt et al.[57] further confirmed that three modes of binding are distinguishable in the silver−DNA binding. The guanine N7 site is a major binding site at Ag/nucleotide concentration ratios between 0.2 and 0.5, while type II involves A−T and G−C base pair sites and often results in proton liberation. Type III is observed when the major binding sites for type I and type II complexes are saturated. Wu et al. also reported[58] that the silver−DNA binding causes the DNA to switch from its B-form structure, which originally is twisted to a flat base pair structure for type I complexes. In type II complexes, the flat base structure switches back to the propeller base pair structure. In their report, Arya and Yang[59] observed that type I complexes are formed from a mixture containing Ag(I) and calf-thymus DNA at a molar ratio of 1:5 and that Ag(I) binds to guanine but not to adenine, cytosine, thymine and the backbone phosphate groups.

Although silver ions bind readily with ligands and molecules as well as proteins in the human body, including albumins and metallothioneins and interact with trace metals in metabolic pathways, silver release occurred at such a relatively slow rate and low concentrations that it does not pose a threat to the human body. Ag^+ has been reported to lead to the uncoupling of the respiratory chain from oxidative phosphorylation, a collapse of the proton motive force across the cytoplasmic membrane, and the interaction with thiol groups of membrane-bound enzymes and proteins.[60−62] The cytoplasmic membrane contains proteins and enzymes vital to the respiratory chain and key transport channels and has been severally suggested as a primary target site for biocidal activity of the silver ion at low concentrations.[60−63] Silver ions interact with cytoplasmic components inside the cell at higher concentrations.[62,63]

The effectiveness of the antibacterial activity of silver ions even when present in low concentrations has been further highlighted in the literature by Rtimi et al.,[64] who explained *E. coli* inactivation in Zr−NO−Ag co-sputtered surfaces through the oligodynamic effect.

We believe that a similar or related mechanism may be operating in the recently described "Zombie killing effect" induced by silver ions in bacteria,[65] also expressed through the equation

$$Ag^+ + \text{viable bacterium} \rightarrow (\text{Ag killed bacterium}) \quad (12)$$

Our current finding on visible-light-activated undoped antimicrobial silver oxide coatings also provides the additional advantage of an improved simple integrated fabrication route based on reactive magnetron sputtering, alongside other significant recent advances based on doped silver nitrides and complex silver oxynitrides, as well as doped titanium dioxide coatings with copper and fluorine using sol and dip coating to prepare a visible-light-activated antimicrobial coating.[2−4] The silver oxide coatings can also be considered for application as a top layer antimicrobial coating for orthopedic implant coatings prepared by magnetron sputtering[66] or other preparation methods.

Clinical microbiologists have observed that bacteria are resistant to silver in a variety of environments and circumstances.[67] The environments include chronic wounds and burns, dentistry, occupational silver exposure, and water systems.[67,68] Evidence of bacterial resistance to silver is provided by mutagenic changes within the bacterial genome.[67] Bacterial resistance to silver can arise due to intrinsic natural properties or through DNA mutations in the plasmid and the transposons.[67] Silver resistance is also transmissible to susceptible bacterial strains. Reports in the literature confirmed the prevalence of epigenetic mechanism during the application of silver nitrate, silver sulphadiazine, or a silver dressing[67] for treatment of wounds indicate that silver ions when present at a concentration lower than 60 ppm preferably bind to albumins, macroglobulins, protein cell membranes of the host, and inorganic anions in the microenvironment and therefore are not available for antimicrobial action.

Silver ion release both in water and saline conducted during this research indicated that the concentrations were lower than 60 ppm, yet Gram-positive and Gram-negative bacteria could not survive on the surfaces for more than 25 min, as observed in the antimicrobial tests conducted. The efficacy of the killing ability in addition to the silver ion release is attributable to the generation of reactive oxygen species, as confirmed by XPS analysis, from photocatalysis and the small sizes of the nanoparticles as evaluated using XRD analysis, which could freely pass through the pores in the bacterial cell membrane resulting in attack on the DNA/RNA, proteins, and the cell membrane simultaneously. This new development in the nanostructured, visible-light-activated photocatalytic silver oxide biomaterial will certainly reactivate further interest of clinicians in managing wound infections and other antimicrobial

DOI: 10.1021/acsomega.9b01856
ACS Omega 2019, 4, 16847−16859

applications since the multiple and simultaneous attack caused by the biomaterial does not give the bacteria time to adjust and initiate resistance when attacked.

4. SUMMARY AND CONCLUSIONS

We prepared an optically transparent mixed-phase but single compound silver oxide thin film biomaterial through the variation of two deposition parameters, namely, the oxygen flow rate and forward power, during reactive magnetron sputter deposition. The undoped silver oxide films can be activated through photocatalysis since their band gap can be tuned to be within the visible range of the solar spectrum, by varying the deposition parameters appropriately. We confirmed the release of silver ions into water and saline solution when our prepared silver oxide films were exposed to these environments. The silver oxide films also displayed antimicrobial properties through rapid bacterial contact killing. The rate of metal ion release and the relative stability of any silver complexes can be controlled using variations in the ligand architecture and the overall structural motif of a silver compound. We observed that there is a significant statistical difference between the logs of colony forming units for each of the Gram-positive and Gram-negative bacteria on the silver oxide-coated substrate compared to that on the two control surfaces of silver-coated and uncoated glass substrates used in this investigation over the time periods considered, implying that the exposure of the microbes to the silver oxide surfaces has an antimicrobial effect on them.

There was however no statistically significant difference in the logs of colony forming units of all four bacteria on the silver oxides deposited at different forward powers used during reactive magnetron sputtering, and all of the silver oxide coatings showed an antimicrobial effect on bacteria exposed to them. The mechanism of antimicrobial activity of the aqueous silver ions released from our silver oxide thin film and the rapid killing of microbes are proposed to take place in three ways, namely, the interference with electron transport, binding to DNA, and interaction with the cell membrane. The coordination of donor atoms to the silver(I) center and the ease of ligand replacement appear to be the key factors leading to a wide spectrum of antimicrobial activities and to be the primary targets for the inhibition of bacterial survival and growth. We believe that the above mechanisms are responsible for the rapid death of bacteria reported in our killing curve investigation on microbes when they are exposed to silver oxide films. A recent (2017) investigation by Rtimi et al.[69] has also confirmed the multiple channels of silver−copper ion bacterial inactivation involving a predominant ionic diffusion route through cell wall porins and surface-effect-dominated cell wall damage in genetically modified bacteria that were free from cell wall porins. The ability of the silver oxide films to also transmit visible light opens the potential for their application beyond the development of antimicrobial surfaces in a hospital environment into other areas like contact lenses and in application areas where both optical transparency and antimicrobial activity are required.

5. EXPERIMENTAL METHODS

5.1. Deposition of Silver and Silver Oxide Thin Films. Thin films of silver oxide were deposited using a cryopumped vacuum chamber by a reactive magnetron sputtering unit. Glass microscope slides were used as substrates for deposition. The glass slides were cleaned ultrasonically using isopropyl alcohol and then washed with deionized water before the deposition of the thin films. A solid silver target of very high purity supplied by PI-KEM (99.99%) was used for deposition, while the sputtering and reactive gases were argon and oxygen, respectively.

5.2. Scanning Electron Microscopy. A Hitachi S4100 field emission scanning electron microscope was used to obtain the scanning electron microscope micrographs during investigation.

5.3. X-ray Diffraction Analysis. A Siemens D5000 X-ray diffractometer using a Cu Kα radiation of wavelength 1.54 nm with Powder Cell software was used for X-ray diffraction analysis. The 2θ angle was varied between 5 and 155°.

5.4. Raman Spectroscopy. Raman spectroscopy, using a laser source of wavelength 532 nm at an energy of 2 mW, was conducted on the deposited samples using a Thermo Scientific DXR Raman microscope spectrometer interfaced with a computer with OMNIC spectra software to obtain the Raman spectra of the as-deposited silver oxide thin films.

5.5. X-ray Photoelectron Spectroscopy. The X-ray photoelectron spectroscopy used for this investigation was performed using a Scientia ESCA300 spectrometer (Thermo Scientific) provided by the National EPSRC User's Services at the University of Newcastle Upon Tyne, U.K. The excitation source is Al Kα with an excitation energy of 1.5 keV and a current of 3 mA. Survey scans were obtained at 200 eV, while 40 eV pass energy was used for the high-resolution regions at 120 and 60 s sweep times. Three different spots of sizes 800 × 400 μm^2 were selected and scanned on each sample. A base pressure of 8×10^{-10} Torr was maintained in the chamber during analysis. Casa XPS software was used for curve fittings. The background subtraction was conducted with the Shirley method. The shapes of the Ag $3d_{5/2}$ and Ag $3d_{3/2}$ peaks were fitted with a Gaussian (30%)−Lorentzian (70%) peak function for all of the spectra analyzed.

5.6. Optical Transmittance, Reflectance, and Band Gap. The optical characterization of the deposited thin films was performed using an Aquila nkd-8000 spectrophotometer. This facility simultaneously collects both transmittance and reflectance spectra using Pro-Optix software. The silver oxides used for this characterization were deposited on glass slides at varying oxygen flow rates and deposition powers each at a deposition time of 2 min. The experiments were carried out in the wavelength range of 350−1100 nm at an incidence angle of 10° for spectral analysis.

5.7. Atomic Absorption Spectroscopy. Silver ion release was monitored using an AAnalyst 300 flame atomic absorption spectrophotometer manufactured by PerkinElmer. All of the operations of the instrument are computer-controlled through a software. Selected samples deposited at 100, 200, 250, 300, 350, and 400 W powers and a 10 sccm oxygen flow rate were used in the study. Each glass microscope slide coated with the silver oxide films was cut into four equal portions; then, an equal amount of either water or saline solution was measured into bottles and each of the pieces was dropped in the bottles and sealed. The silver oxide surfaces were removed after 1, 6, 12, or 24 h contact with water and saline solution and used to evaluate silver ion release.

5.8. Antimicrobial Tests and Killing Curves for Microbes. Four microbes were selected for conducting the antimicrobial tests in this research, namely, *E. coli* and *P. aeruginosa* (Gram-negative) and *S. epidermidis* and *S. aureus* (Gram-positive). Overnight bacterial cultures were grown in Luria broth (LB) media. Ten milliliters of the LB was pipetted out into sterile bottles into which bacteria were inoculated using an inoculation loop sterilized by Bunsen flame and shaken at a

DOI: 10.1021/acsomega.9b01856
ACS Omega 2019, 4, 16847−16859

speed of 150 rpm at 37 °C overnight. Then, 4.8 g of agar powder was measured and out into a bottle. Furthermore, 10 g of Luria broth powder was measured and added into the same bottle containing the agar. Then, 400 mL of distilled water was used to prepare a solution after gentle shaking. The bottle and contents were autoclaved at 121 °C for 15 min. The prepared nutrient agar was cooled slightly to the handling temperature of the plate. The agar was plated in the Petri dishes and allowed to cool and dry to be ready for culturing bacteria. The inoculation loop was sterilized using the Bunsen burner blue flame before and after use. Tips and other containers used during the preparation of the material and testing were autoclaved at 121 °C for 15 min before further using them.

Silver oxides were deposited at different conditions of forward power and oxygen flow rate on glass microscope slides to test their antimicrobial activity. A pure silver thin film prepared by magnetron sputtering at 300 W forward power and glass microscope slides, both washed ultrasonically, were used as control samples. The bacterial cells were harvested from the overnight culture that was incubated at 37 °C and suspended in sterile phosphate-buffered saline (PBS). Then, 10 mL of the cell suspension was pipetted out into an Eppendorf tube and vortexed after washing twice in PBS. The optical density of the microbes was measured at 570 nm, and the suspensions were diluted using PBS to desired values (0.15 for *E. coli* and 0.2 for *S. aureus*, *S. epidermidis*, and *P. aeruginosa*). Furthermore, 20 μL of the bacterial suspension was pipetted out and dropped on the silver oxide, silver, and glass slide surfaces and allowed to interact with the surfaces for 0, 5, 10, 15, 20, 25, 30, 60, and 90 min. After each time interval, sterile swaps were used to remove the microbes from the surfaces and added into 1 mL of PBS within 10 s. The microbes were removed from the swaps by vortexing for 20 s and sonicating for 5 min. A serial dilution of the bacterial suspension was done using sterile distilled water, and 50 μL of the desired diluent's (first, second, third or fourth, fifth and sixth) of the bacteria were dropped at three points on each portion of the Petri dishes on which agar has been prepared. The plated Petri dishes were cultured overnight in an incubator at 37 °C, and the colony forming units (CFU) were counted using the Miles and Misra method. The log of CFU was plotted against time to present the killing curves.

5.9. Statistical Analysis. The IBM SPSS statistics software package, version 24 (IBM Corp, New York), was used for data analysis with the results expressed as mean ± standard deviation. The microbial colonization on the surfaces is expressed in terms of the colony forming units (CFU) as $\log_{10}$ CFU for the four microbes tested. The Student *t*-test was used to compare the effects of the variations in the conditions, i.e., forward power during reactive magnetron sputtering used to prepare the silver oxide-coated substrate surfaces ($p < 0.05$) and the microbial colonization over time. A one-way ANOVA test was used to compare the microbial colonization over time on the silver oxide-coated substrate surfaces with that on the two control surfaces of silver-coated and uncoated glass substrates. The post hoc Tukey test was used to determine the statistical significance of the test ($p < 0.05$). The Levene test for equality of variance was used to determine which data set should be used to interpret the results obtained in each case.

AUTHOR INFORMATION

Corresponding Author

*E-mail: Nathaniel.Tsendzughul@uws.ac.uk.

ORCID

Nathaniel T. Tsendzughul: 0000-0002-0926-7313

Author Contributions

A.A.O. developed the concept of the research and designed the experimental setup for the acquisition of the data, as well as the analysis and interpretation of the data, while N.T.T. (doctoral researcher) carried out the experimental measurements as well as the interpretation of the data. The antimicrobial tests were conducted by N.T.T. A.A.O. and N.T.T. both drafted the article, revised it critically for important intellectual content, and finally approved the version of the manuscript to be published.

Notes

The authors declare no competing financial interest.

The tests reported in this paper did not involve any human or animal investigation.

All of the data in this investigation have been reported in the paper and are freely available.

ACKNOWLEDGMENTS

We would like to acknowledge Charles McGinnis of the Chemistry group of the university for support with the use of the atomic absorption spectroscopy facility. We also acknowledge Prof. Craig Williams and Dr. William Mackay for the design, development, experimental setup, and data acquisition of the antimicrobial tests with N.T.T. and A.A.O.

REFERENCES

(1) Byrne, J. A.; Dunlop, P. S.; Hamilton, J. W.; Fernandez-Ibanez, P.; Polo-Lopez, I.; Sharma, P. K.; Vennard, A. S. A review of heterogenous photocatalysis for water and surface disinfection. *Molecules* **2015**, *20*, 5574−5615.

(2) Ritmi, S.; Pulgarin, C.; Kiwi, J. Uniform, Adhesive, and Low Cytotoxic Films Accelerating Bacterial Reduction in the Dark and under Visible Light. In *Thin Film Coatings for Biomaterials and Biomedical Applications*; Griesser, H. J., Eds.; Woodhead Publishing Series in Biomaterials; Woodhead Publishing, 2016; Chapter 10, pp 289−294.

(3) Ritmi, S. Indoor light enhanced photo-catalytic ultra-thin films on flexible non-heat resistant substrates reducing bacteria infection rates. *Catalysts* **2017**, *7*, No. 57.

(4) Leyland, N. S.; Podporska-Carroll, J.; Browne, J.; Hinder, S. J.; Quilty, B.; Pillai, S. C. Highly efficient, Cu doped TiO_2 anti-bacterial visible light active photocatalytic coatings to combat hospital acquired infections. *Sci. Rep.* **2016**, *6*, No. 24770.

(5) lippard, S. J.; Berg, J. M. *Principles of Bioinorganic Chemistry*, 4th ed.; University Science Books: Mill Valley, CA, 1994; pp 1−73.

(6) Fenton, D. E. *Biocoordination Chemistry*, 2nd ed.; Oxford Chemistry Primers: New York, 1995; pp 1−59.

(7) Bertini, I.; Gray, H. B.; Lippard, S. J.; Valentine, J. S. *Bioinorganic Chemistry*, 1st ed.; University Science Books: Sausalito, CA, 1994; pp 1−35, 315−444.

(8) Morones, J. R.; Elechiguerra, J. L.; Camacho, A.; Holt, K.; Kouri, J. B.; Ramírez, J. T.; Yacaman, M. J. The bactericidal effect of silver nanoparticles. *Nanotechnology* **2005**, *16*, 2346−2353.

(9) Jung, W. K.; Koo, H. C.; Kim, K. W.; Shin, S.; Kim, S. H.; Park, Y. H. Antibacterial activity and mechanism of action of the silver ion in *Staphylococcus aureus* and *Escherichia coli*. *Appl. Environ. Microbiol.* **2008**, *74*, 2171−2178.

(10) Bury, N. R.; Wood, C. M. Mechanism of branchial apical silver uptake by rainbow trout is via the proton-coupled Na(+) channel. *Am. J. Physiol.: Regul., Integr. Comp. Physiol.* **1999**, *277*, R1385−1391.

(11) Choi, O.; Deng, K. K.; Kim, N. J.; Ross, L.; Surampalli, R. Y.; Hu, Z. The inhibitory effects of silver nanoparticles, silver ions, and silver chloride colloids on microbial growth. *Water Res.* **2008**, *42*, 3066−3074.

DOI: 10.1021/acsomega.9b01856
ACS Omega 2019, 4, 16847−16859

(12) Vermeulen, H.; van Hattem, J. M.; Storm-Versloot, M. N.; Ubbink, D. T.; Westerbos, S. J. Topical silver for treating infected wounds. *Cochrane Database Syst. Rev.* **2007**, No. CD005486.
(13) Meng, F.; Sun, Z. A mechanism for enhanced hydrophilicity of silver nanoparticles modified TiO_2 thin films deposited by RF magnetron sputtering. *Appl. Surf. Sci.* **2009**, *255*, 6715−6720.
(14) Gao, X. Y.; Wang, S. Y.; Li, J.; Zheng, Y. X.; Zhang, R. J.; Zhou, P.; Yang, Y. M.; Chen, L. Y. Study of structure and optical properties of silver oxide films by ellipsometry, XRD and XPS methods. *Thin Solid Films* **2004**, *455*−*456*, 438−442.
(15) Bancroft, G. M.; Chan, T.; Puddephatt, R. J.; Tse, J. S. Role of the Au 5d orbitals in bonding: Photoelectron spectra of [AuMe (PMe3)]. *Inorg. Chem.* **1982**, *21*, 2946−2949.
(16) Grass, G.; Rensing, C.; Solioz, M. Minireviews metallic copper as an antimicrobial surface. *Appl. Environ. Microbiol.* **2011**, *77*, 1541−1547.
(17) Wilks, S. A.; Michels, H.; Keevil, C. W. The survival of *Escherichia coli* O157 on a range of metal surfaces. *Int. J. Food Microbiol.* **2005**, *105*, 445−454.
(18) Lazar, V. Quorum sensing in biofilms - How to destroy the bacterial citadels or their cohesion/power. *Anaerobe* **2011**, *17*, 280−285.
(19) Naraginti, S.; Sivakumar, A. Eco-friendly synthesis of silver and gold nanoparticles with enhanced bactericidal activity and study of silver catalyzed reduction of 4-nitrophenol. *Spectrochim. Acta, Part A* **2014**, *128*, 357−362.
(20) Wu, D.; Fan, W.; Kishen, A.; Gutmann, J. L.; Fan, B. Evaluation of the antibacterial efficacy of silver nanoparticles against Enterococcus faecalis biofilm. *J. Endod.* **2014**, *40*, 285−290.
(21) Periasamy, S.; Joo, H. S.; Duong, A. C.; Bach, T. H. L.; Tan, V. Y.; Chatterjee, S. S.; Cheung, G. Y. C.; Otto, M. How *Staphylococcus aureus* biofilms develop their characteristic structure. *Proc. Natl. Acad. Sci. U.S.A.* **2012**, *109*, 1281−1286.
(22) Pelaez, M.; Nolan, N. T.; Pillai, S. C.; Seery, M. K.; Falaras, P.; Kontos, A. G.; Dunlop, P. S. M.; Hamilton, J. W. J.; Byrne, J. A.; O'shea, K.; Entezari, M. H.; Dionysiou, D. D. A review on the visble light active TiO_2 photocatalysts for environmental applications. *Appl. Catal., B* **2012**, *125*, 331−349.
(23) Dunlop, P. S. M.; Sheeran, C. P.; Byrne, J. A.; MacMahon, M. A. S.; Boyle, M. A.; MacGuigan, K. G. Inactivation of clinically relevant pathogens by photocatalytic coatings. *J. Photochem. Photobiol., A* **2010**, *216*, 303−310.
(24) Seery, M. K.; George, R.; Floris, P.; Pillai, S. C. Silver doped titanium dioxide nanomaterials for enhanced visible light photocatalysis. *J. Photochem. Photobiol., A* **2007**, *189*, 258−263.
(25) Wei, Q.-Y.; Xiong, J.-J.; Jiang, H.; Zhang, C.; Ye, W. The antimicrobial activities of the cinnamaldehyde adducts with amino acids. *Int. J. Food Microbiol.* **2011**, *150*, 164−170.
(26) Li, Y.; Xue, Y.; Tian, J.; Song, X.; Zhang, X.; Wang, X.; Cui, H. Silver oxide decorated graphitic carbon nitride for the realization of photocatalytic degradation over the full solar spectrum: From UV to NIR region. *Sol. Energy Mater. Sol. Cells* **2017**, *168*, 100−111.
(27) Mazierski, P.; Malankowska, A.; Kobylanski, M.; Diak, M.; Kozak, M.; Winiarski, M. J.; Klimczuk, T.; Lisowski, W.; Nowaczyk, G.; Zaleska-Medynska, A. Photcatalytically active TiO_2/AgO_2 nanotube arrays interfaced with silver nanoparticles obtained from the one-step anodic oxidation of Ti-Ag alloys. *ACS Catal.* **2017**, *7*, 2753−2764.
(28) Chen, H. L.; Yang, Z. H.; Lee, S. Observation of surface coverage-dependent surface-enhanced Raman scattering and the kinetic behaviour of methyl blue adsorbed on silver oxide nanocrystallites. *Langmuir* **2016**, *32*, 10184−10188.
(29) Tsendzughul, N.; Ogwu, A. A.; Mirzaeian, M.; Williams, C.; McKay, W. In *Anti-microbial Silver Oxide Films with Rapid Bacteria Contact Killing*, Presented at the 44th International Conference on Metallurgical Coatings and Thin Films, ICMCTF 2017, San Diego, California, April 24−28, 2017.
(30) Jiang, W.; Wang, X.; Wu, Z.; Yue, X.; Yuan, S.; Lu, H.; Liang, B. Silver oxide as superb and stable photocatalyst under visible and near-infrared light irradiation and its photocatalytic mechanism. *Ind. Eng. Chem. Res.* **2015**, *54*, 832−841.
(31) Dellasega, D.; Casari, C. S.; Vario, F.; Conti, C.; Bottani, C. E.; Bassi, A. L. Nanostructured Ag_4O_4 thin films produced by ion beam oxidation of silver. *Appl. Surf. Sci.* **2013**, *266*, 161−169.
(32) Dellasega, D.; Facibeni, A.; Di Fonzo, F.; Bogana, M.; et al. Nanostructured Ag_4O_4 films with enhanced antibacterial activity. *Nanotechnology* **2008**, *19*, No. 475602.
(33) Waterhouse, G. I. N.; Bowmaker, G. A.; Metson, J. B. The thermal decomposition of silver (I, III) oxide: A combined XRD, FT-IR and Raman spectroscopic study. *Phys. Chem. Chem. Phys.* **2001**, *3*, 3838−3845.
(34) Langford, J. I.; Wilson, A. J. C. Scherrer after sixty years: A survey and some new results in the determination of crystallite size. *J. Appl. Crystallogr.* **1978**, *11*, 102−113.
(35) http://www.casaxps.com/help_manual/manual_updates/Basics_Quantification_of_XPS_Spectra.pdf (accessed Sept 18, 2015).
(36) http://www.mercury-instruments.com/index.html (accessed Nov 15, 2016).
(37) Goderecci, S.; Kaiser, E.; Yanakas, M..; Norris, Z.; Scaturro, J.; Oszust, R.; Medina, C.; Waechter, F.; Heon, M.; Krchnavek, R.; Yu, L.; Lofland, S.; Demarest, R.; Caputo, G.; Hettinger, J. Silver oxide coatings with high silver-ion elution rates and characterization of bactericidal activity. *Molecules* **2017**, *22*, No. 1487.
(38) Bukhtiyarov, V. I.; Boronin, A. I.; Savchenko, V. I. Stages in the modification of a silver surface for catalysis of the partial oxidation of ethylene: I. Action of Oxygen. *J. Catal.* **1994**, *150*, 262−267.
(39) Campbell, C. T. Atomic and molecular oxygen adsorption on Ag(111). *Surf. Sci.* **1985**, *157*, 43−60.
(40) Bukhtiyarov, V. I.; Kondratenko, V. A.; Boronin, A. I. Features of the interaction of a CO + O_2 mixture with silver under high pressure. *Surf. Sci.* **1993**, *293*, L826−L829.
(41) Altass, H.; Carley, A. F.; Davies, P. R.; Davies, R. J. XPS and STM studies of the oxidation of hydrogen chloride at Cu(100) surfaces. *Surf. Sci.* **2016**, *650*, 177−186.
(42) Waterhouse, G. I. N.; Bowmaker, G. A.; Metson, J. B. Interaction of a polycrystalline silver powder with ozone. *Surf. Interface Anal.* **2002**, *33*, 401−409.
(43) Khakpoor, A. A.; Borjian, R.; Hoseinzade, M. Optical properties improvement TiO_2 thin films with adding the Au, Ag or Cu Nanoparticles. *Int. Mater. Phys. J.* **2013**, *1*, 8−13.
(44) Mardare, D.; Tasca, M.; Delibas, M.; Rusu, G. I. On the structural properties and optical transmittance of TiO_2 r.f. sputtered thin films. *Appl. Surf. Sci.* **2000**, *156*, 200−206.
(45) Ogwu, A. A.; Bouquerel, E.; Ademosu, O.; Moh, S.; Crossan, E.; Placido, F. An extended Derjaguin-Landau-Verwy-Overbeek theory approach to determining the surface energy of copper oxide thin films prepared by reactive magnetron sputtering. *Metall. Mater. Trans. A* **2005**, *36*, 2435−2439.
(46) Wang, G.; Ma, X.; Huang, B.; Cheng, H.; Wang, Z.; Zhan, J.; Qin, X.; Zhang, X.; Dai, Y. Controlled synthesis of Ag_2O microcrystals with facet-dependent photocatalytic activities. *J. Mater. Chem.* **2012**, *22*, 21189−21194.
(47) Wang, X.; Li, S.; Yu, H.; Yu, J.; Liu, S. Ag_2O as a new visible-light photocatalyst: Self-stability and high photocatalytic activity. *Chem. − Eur. J.* **2011**, *17*, 7777−7780.
(48) Chen, Y. J.; Chiang, Y. W.; Huang, M. H. Synthesis of diverse Ag_2O crystals and their facet-dependent photocatalytic activity examination. *ACS Appl. Mater. Interfaces* **2016**, *8*, 19672−19679.
(49) Money, N. P. Measurement of pore size in the hyphal cell wall of *Achlya bisexualis*. *Exp. Mycol.* **1990**, *14*, 234−242.
(50) Berestovsky, G. N.; Ternovsky, V. I.; Kataev, A. A. Through pore diameter in the cell wall of *Chara corallina*. *J. Exp. Bot.* **2001**, *52*, 1173−1177.
(51) Bard, A. J.; Holt, K. B. Interaction of silver(I) ions with the respiratory chain of *Escherichia coli*: An electrochemical and scanning electrochemical microscopy study of the antimicrobial mechanism of micromolar Ag^+. *Biochemistry* **2005**, *44*, 13214−13223.

DOI: 10.1021/acsomega.9b01856
ACS Omega 2019, 4, 16847−16859

(52) Feng, Q. L.; Wu, J.; Chen, G. Q.; Cui, F. Z.; Kim, T. N.; Kim, J. O. A mechanistic study of the antibacterial effect of silver ions on *Escherichia coli* and *Staphylococcus aureus*. *J. Biomed. Mater. Res.* **2000**, *52*, 662−668.
(53) Mcdonnell, G.; Russell, A. D. Antiseptics and disinfectants: Activity, action, and resistance. *Clin. Microbiol. Rev.* **1999**, *12*, 147−179.
(54) Bromberg, L. E.; Braman, V. M.; Rothstein, D. M.; Spacciapoli, P.; O'Connor, S. M.; Nelson, E. J.; Buxton, D. K.; Tonetti, M. S.; Friden, P. M. Sustained release of silver from periodontal wafers for treatment of periodontitis. *J. Controlled Release* **2000**, *68*, 63−72.
(55) Tajmir-Riahi, H. A.; Arakawa, H.; Neault, J. F. Silver(I) complexes with DNA and RNA studied by Fourier transform infrared spectroscopy and capillary electrophoresis. *Biophys. J.* **2001**, *81*, 1580−1587.
(56) Dixit, V. Synthesis, Characterisation and Antimicrobial Activity of Novel Phosphine Stabilized Silver(I) Dicarboxylate Complexes. Ph.D. Thesis, Dublin institute of Technology, 2010.
(57) Izatt, R. M.; Christensen, J. J.; Rytting, J. H. Sites and thermodynamic quantities associated with proton and metal ion interaction with ribonucleic acid, deoxyribonucleic acid, and their constitutent bases, nucleosides, and nucleotides. *Chem. Rev.* **1971**, *71*, 439−481.
(58) Wu, H. M.; Dattagupta, N.; Crothers, D. M. Solution structural studies of the A and Z forms of DNA. *Proc. Natl. Acad. Sci. U.S.A.* **1981**, *78*, 6808−6811.
(59) Arya, S. K.; Yang, J. T. Optical rotatory dispersion and circular dichroism of silver(I): Polyribonucleotide complexes. *Biopolymers* **1975**, *14*, 1847−1861.
(60) Schreurs, W. J. A.; Rosenburgh, H. Effect of silver ions on transport and retention of phosphate by *Escherichia coli*. *J. Bacteriol.* **1982**, *152*, 7−13.
(61) Liau, S. Y.; Read, D. C.; Pugh, W. J.; Furr, J. R.; Russell, A. D. Interaction of silver nitrate with readily identifiable groups: relationship to the antimicrobial actions of silver ions. *Lett. Appl. Microbiol.* **1997**, *25*, 279−283.
(62) Zeiri, L.; Bronk, B. V.; Shabtai, Y.; Eichler, J.; Efrim, S. A. Surface-enhanced Raman spectroscopy as a tool for probing specific biochemical components in bacteria. *Appl. Spectrosc.* **2004**, *58*, 33−40.
(63) Bragg, P. D.; Rainnie, D. J. The effect of silver ions on the respiratory chain of *Escherichia coli*. *Can. J. Microbiol.* **1974**, *20*, 883−889.
(64) Rtimi, S.; Pascu, M.; Sanjines, R.; Pulgarin, C.; Ben-Simon, M.; Houas, A.; Lavanchy, J. C.; Kiwi, J. Zr-NO-Ag co-sputtered surfaces leading to *E. coli* inactivation under actinic light. Evidence for the oligodynamic effect. *Appl. Catal., B* **2013**, *138−139*, 113−121.
(65) Wakschlak, R. B.-K.; Pedahzur, R.; Avnir, D. Antibacterial activity of silver-killed bacteria: the "Zombie effect". *Sci. Rep.* **2015**, *5*, No. 9555.
(66) Oje, A. M.; Ogwu, A. A. Chromium oxide coatings with the potential for eliminating the risk of chromium ion release in orthopaedic implants. *R. Soc. Open Sci.* **2017**, *4*, No. 170218.
(67) Lansdown, A.; Williams, A. Bacterial resistance to silver-based antibiotics. *Nurs. Times* **2007**, *103*, 48−49.
(68) Davis, H. R.; Mullany, P. Isolation of silver and antibiotic-resistant Enterobacter cloacae from teeth. *Oral Microbiol. Immunol.* **2005**, *20*, 191−194.
(69) Rtimi, S.; Nadtochenko, V.; Khmel, I.; Kiwi, J. Evidence for differentiated ionic and surface contact effects during bacterial inactivation by way of genetically modified bacteria. *Chem. Commun.* **2017**, *53*, 9093−9096.

DOI: 10.1021/acsomega.9b01856
ACS Omega 2019, 4, 16847−16859